Journal of
MARINE RESEARCH

Volume 34, Number 3

The role of inertia-gravity and planetary waves in the response of a tropical ocean to the incidence of an equatorial Kelvin wave on a meridional boundary

by D. L. T. Anderson[1] and P. B. Rowlands[1]

ABSTRACT

The problem of an equatorial Kelvin wave of step-function form incident on an eastern meridional boundary is solved on an equatorial beta-plane. The nature of the transient planetary and inertia-gravity waves is examined and the way in which they combine to produce a coastally trapped Kelvin wave evaluated.

It is shown that the coastal wave in the vicinity of the head of the disturbance amplifies like $y^{\frac{1}{2}}$ where y is the distance from the equator, but that in the wake of this head, the upwelling is reduced to $1/\sqrt{2}$ that of the incoming equatorial Kelvin wave. Planetary waves lead to a westward broadening of the upwelling field, most rapid near the equator. Inertia-gravity waves, particularly that of the lowest horizontal mode, can lead to frontogentic effects but do not induce any mean upwelling.

An approximate theory eliminating the inertia-gravity waves is then considered which, it is shown, represents well the coastal propagation as well as the westward propagation of planetary waves.

1. Introduction

Much work has recently been done on the theory of coastal upwelling in the oceans, a phenomenon of considerable relevance to the fishing industry, as fish tend to congregate in regions of upwelling to feed on the nutrients brought up from the

1. Department of Applied Mathematics and Theoretical Physics, University of Cambridge, Silver Street, Cambridge, CB3 9EW, England.

deep ocean. For the important meteorological time scales of a few days the dynamics of upwelling are generally associated with the propagation of internal Kelvin waves along a coast (e.g. Walin, 1972). Yoshida (1959) showed that similar gravity waves can occur in the tropics where they propagate along the equator and are confined to low latitudes; subsequently Ichiye (1959) demonstrated the possibility of low frequency Rossby waves also trapped near the equator. Moore (1968), for a basin with north–south boundaries and harmonic time dependence, showed how eastward traveling equatorial Kelvin waves generate at the eastern boundary equatorial waves reflected back toward the west and coastal Kelvin waves propagating away from the equator. His results are supported by numerical calculations by Mofjeld and Rattray (1971) of the normal modes of oscillation of a rectangular basin centered at the equator. The connection between equatorial waves and coastal Kelvin waves is qualitatively obvious in Mofjeld and Rattray's diagrams.

The problem solved in this paper is that of a step-function equatorial Kelvin wave incident on an eastern coast. The form of the coastal Kelvin wave generated is calculated at the coast for (a) the exact problem and (b) a problem in which an approximation is made to eliminate high frequency waves. It is shown that it is possible to derive an approximation which gives results in good agreement with the exact solution.

2. Formulation

Following Lighthill (1969), we represent the effect of a wind stress applied at the ocean surface as a body force uniformly distributed through the upper mixed layer. Then, using the notation of Gill and Clarke (1974), we separate off the vertical dependence of the linearized equations in the usual way and nondimensionalize the variables with the length scale $a_n = (c_n/2\beta)^{\frac{1}{2}}$ (the "equatorial radius of deformation" of Gill and Clarke (op. cit.)) and the time scale a_n/c_n, where c_n is the speed of propagation of gravity waves in the nth vertical mode in the absence of rotation (Bretherton, 1965). The resulting equations are

$$u_t - \tfrac{1}{2} y v + p_x = X \tag{2.1}$$

$$v_t + \tfrac{1}{2} y u + p_y = Y \tag{2.2}$$

$$p_t + u_x + v_y = 0 \tag{2.3}$$

where (ignoring the vertical structure functions)

u is the zonal component of velocity,
v is the meridional component of velocity,
p is the pressure perturbation divided by density,
(X,Y) is the body force which is postulated to cause the fluid motion,
x, y, are zonal and meridional co-ordinates with $y = 0$ at the equator,
t is the time,

and a suffix denotes differentiation.

The y-dependence can be separated out of equations (2.1)-(2.3) by expanding the dependent variables and the forcing terms as series of parabolic cylinder functions. Thus,

$$F = \sum_{m=0}^{\infty} F^m(x,t)\, D_m(y) \tag{2.4}$$

where F is any dependent variable and $D_m(y)$ is the parabolic cylinder function of order m (Abramowitz and Stegun, 1965, Ch. 19). Following Gill (1975) it is now convenient to define two new dependent variables:

$$q = p + u \tag{2.5}$$

and

$$r = p - u \tag{2.6}$$

Expanding q and r as in (2.4) and using the orthogonality of the parabolic cylinder functions and the recurrence relations

$$\frac{dD_m}{dy} + \tfrac{1}{2} y D_m = m D_{m-1} \tag{2.7}$$

and

$$\frac{dD_m}{dy} - \tfrac{1}{2} y D_m = - D_m + 1 \tag{2.8}$$

we obtain the following set of equations after eliminating v^m:

$$q^0{}_t + q^0{}_x = X^0 \tag{2.9}$$

$$2q^1{}_{tt} + 2q^1{}_{xt} + q^1 = 2X^1{}_t + 2Y^0 \tag{2.10}$$

$$\begin{aligned} 2q^{m+2}{}_{ttt} - 2q^{m+2}{}_{xxt} + (2m+3)\, q^{m+2}{}_t - q^{m+2}{}_x &= 2X^{m+2}{}_{tt} - 2X^{m+2}{}_{xt} \\ &+ (m+1)\, X^{m+2} - X^m + 2Y^{m+1}{}_t - 2Y^{m+1}{}_x \end{aligned} \tag{2.11}$$

$$\begin{aligned} 2r^m{}_{ttt} - 2r^m{}_{xxt} + (2m+3) r^m{}_t - r^m{}_x &= 2X^m{}_{tt} - 2X^m{}_{xt} + (m+1)(m+2) X^{m+2} \\ &- (m+2) X^m - 2(m+1) Y^{m+1}{}_t - 2(m+1) Y^{m+1}{}_x \end{aligned} \tag{2.12}$$

$$(m+1) q^{m+2}{}_t + (m+1) q^{m+2}{}_x + r^m{}_t - r^m{}_x = (m+1) X^{m+2} - X^m \tag{2.13}$$

all for $m > 0$.

Instead of (2.13) we will often use the equivalent equation

$$2q^{m+2}{}_{tt} + 2q^{m+2}{}_{xt} + (m+2)\, q^{m+2} - r^m = 2X^{m+2}{}_t + 2Y^{m+1}. \tag{2.14}$$

The boundary condition at the eastern wall ($x = 0$) is $u = 0$ which can be partially expressed as

$$q^m = r^m. \tag{2.15}$$

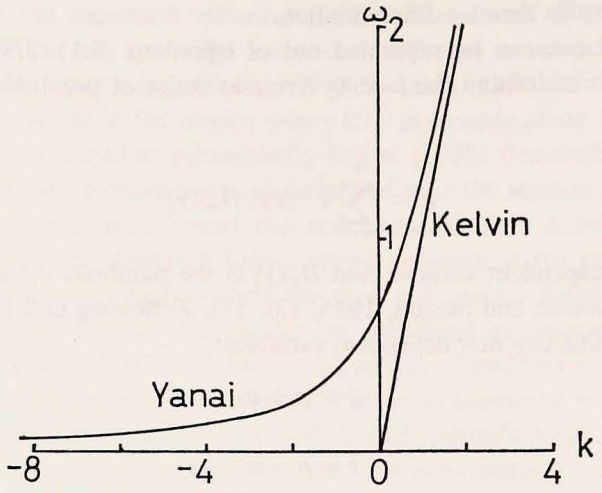

Figure 1. Dispersion curves for Yanai and Kelvin waves in the exact case.

It is apparent from (2.13) and (2.15) that the modes with m even and those with m odd are not coupled and thus that the original problem divides into two separate problems. We will consider primarily the case of even m, which will (§3) be seen to be the more important case. The problem with odd m is analogous.

3. Unforced wave solutions

In this section we briefly recall the dispersion relations for free equatorial waves given by Blandford (1966), as interpretation of many of the later results requires some knowledge of the dispersion properties of free equatorial waves.

If the substitutions

$$q^m \propto e^{-i(\omega t - kx)}, r^m \propto e^{-i(\omega t + kx)} \tag{3.1}$$

are made in the unforced forms of equations (2.9)-(2.12) we obtain for q^0:

$$\omega - k = 0. \tag{3.2}$$

This is the equatorial Kelvin wave and (3.2) shows that it is nondispersive and travels with group and phase velocities equal to unity in our nondimensional units, both eastward. For q^1 we obtain

$$k = \omega - \frac{1}{2\omega} . \tag{3.3}$$

This is sometimes called the Yanai wave (Yanai and Maruyama, 1966), or alternatively mixed Rossby-gravity wave because for low frequencies it has the properties of a Rossby wave and for high frequencies it has the properties of a gravity wave. This wave also has eastward group velocity for all frequencies. The dispersion relations (3.2) and (3.3) are plotted in Fig. 1, where it can be seen that for all fre-

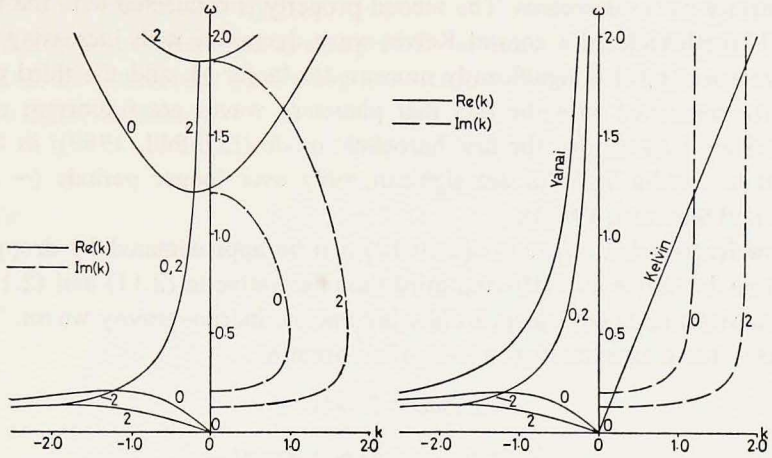

Figure 2. (left) Dispersion curves for r^0 and r^2 (or q^2 and q^4) in the exact case. The curves labelled '0' are for r^0 and those labelled '2' for r^2.

Figure 3. (right) Dispersion curves in the approximate case for Yanai and Kelvin waves, and for r^0 and r^2 (or q^2 and q^4). The curves labelled '0' are for r^0 and those labelled '2' are for r^2. Comparison should be made with Fig. 2. For low frequencies the dispersion curves are similar. For high frequencies inertia-gravity waves are excluded in the approximate case and replaced by trapped waves.

quencies the group velocity of the Yanai wave is less than that of the Kelvin wave. For the low frequencies which are of interest here the equatorial Kelvin wave generated by some remote disturbance will reach the eastern boundary long before the Yanai wave. This is why, as noted in §2, we concentrate mainly on the case of even m in this paper.

Equations (2.11) for q^{m+2} and (2.12) for r^m have the dispersion relation

$$2\omega^3 - 2\omega k^2 - (2m+3)\,\omega - k = 0. \tag{3.4}$$

Solving this for k we find

$$k = -1/4\omega \pm [1/16\omega^2 - (m+3/2) + \omega^2]^{\frac{1}{2}}. \tag{3.5}$$

For sufficiently large ω the square root is real and we have inertia-gravity waves. Similarly, for sufficiently small ω the square root is again real and we have free planetary waves. However, for intermediate frequencies the square root is imaginary and the disturbance decays exponentially in either the positive or negative zonal direction. Thus disturbances with such frequencies can exist only in the neighborhood of a meridional coast, and as shown later a suitable sum of such disturbances constitutes the coastal Kelvin wave. The dispersion curves for equation (3.4) are drawn in Fig. 2 for the modes $m = 0$, 2; the mode $m = 1$ lies between these two. For increasing m it is seen that the range of frequencies where k is complex increases, the imaginary part of k, at fixed ω, increases, and the group velocity of

long planetary waves decreases. The second property is connected with the fact that the zonal length-scale of a coastal Kelvin wave decreases with increasing latitude (as m increases $D_m(y)$ is significantly nonzero for larger y), and the third property is similarly connected with the fact that planetary waves are important on short time-scales ($\sim$ 1 month for the first baroclinic mode (Lighthill, 1969)) in low latitudes but in middle latitudes are signicant only over longer periods ($\sim$ decades (Veronis and Stommel, 1956)).

For low frequencies, equations (2.10-12) can be approximated by dropping the second time derivative in (2.10) and third time derivative in (2.11) and (2.12). This later approximation is equivalent to filtering out the inertia–gravity waves. The dispersion relations corresponding to (3.3), (3.4) are now

$$2\omega k + 1 = 0 \tag{3.6}$$

$$2\omega k^2 + (2m+3)\,\omega + k = 0 \tag{3.7}$$

while that for the Kelvin wave (3.2) remains unchanged.

These dispersion relations are plotted in Fig. 3. Comparison of this figure with Figs. 1 and 2 shows that the equatorial Kelvin wave remains unchanged, the planetary waves are almost unchanged as also are the waves which are confined near a coast, for frequencies below 0.5 in our units. However, the inertia-gravity waves have been replaced by trapped waves; i.e. k is now complex at inertia-gravity wave frequencies. The Yanai wave is virtually unchanged at low frequencies, where it behaves like a planetary wave, but it is considerably changed at high frequencies where it previously had the properties of an inertia-gravity wave. From this free mode analysis one would conclude that the low frequency approximation as applied here is a good approximation for periods long compared not with $1/f$ but with 4π (i.e. the period at which $\omega = 0.5$). In dimensional units for the first baroclinic mode ($c_1 \cong 2ms^{-1}$) $\omega = 0.5$ corresponds to a period of about 12 days. For higher modes c_n is lower and this period is longer; for the baratropic mode this period is about 1 day.

4. An equatorial Kelvin wave incident on an eastern coast (exact solution)

We now consider a particular solution to equations (2.9)-(2.13), namely the response of the model ocean to the arrival of a step-function equatorial Kelvin wave at the east coast. As there is no force acting on the fluid in this case, equations (2.9), (2.11)-(2.14) have their right–hand sides replaced by zero. As equatorial Kelvin waves have eastward group velocity the only solution of (2.9) relevant to the problem of an eastern coast is the incident wave. This will be taken to have the form $q = H(t - x)$ where $H(\theta) = 1$ for $\theta > 0$ and 0 for $\theta < 0$. The response to any more general form of incident wave can be calculated from the response to this wave by convolution.

5. The solution for r^0

The first step in the solution to this problem is to evaluate r^0 using (2.12), (2.15) and the assumed form of q^0. Taking Laplace transforms of these equations and using the initial conditions

$$r^0 = 0 \qquad \text{for } t < 0 \tag{5.1}$$

we obtain

$$-s^3 \hat{r}^0 + s\,\hat{r}^0_{xx} - 3/2\, s\,\hat{r}^0 + \tfrac{1}{2}\,\hat{r}^0_x = 0 \qquad (x < 0) \tag{5.2}$$

and

$$\hat{r}^0 = 1/s \text{ at } x = 0, \tag{5.3}$$

where

$$\hat{r}^0 = \int_0^\infty r^0\, e^{-st} dt. \tag{5.4}$$

The solution of (5.1) and (5.2) is

$$\hat{r}^0 = \frac{1}{s} \exp(k_+ x) \tag{5.5}$$

where

$$k_+ = -1/4s + \left(\frac{1}{16s^2} + 3/2 + s^2\right)^{\frac{1}{2}} \tag{5.6}$$

and the branch of k_+ is chosen so that k_+ is positive for s real and positive. From the inversion theorem for Laplace transforms we then have

$$r^0 = (2\pi i)^{-1} \int_\Gamma s^{-1} \exp(k_+ x + st) ds \tag{5.7}$$

where Γ is the Bromwich contour. The singularities of the integrand are a simple pole at the origin and branch points at $s = \pm i\alpha$ and $\pm i\beta$ where $\alpha = .2071$ and $\beta = 1.2071$ are the positive roots of

$$16\xi^4 - 24\,\xi^2 + 1 = 0 \tag{5.8}$$

Branch cuts are taken from $i\alpha$ to $i\beta$ and from $-i\alpha$ to $-i\beta$ along the imaginary axis. For $t + x > 0$, Γ may be completed by a large semicircle in the negative half-space and by Jordan's lemma the integral around this semicircle will be negligible. The resulting closed contour may then be contracted around the singularities and the integral (5.7) evaluated as

$$r^0 = \left\{1 + \frac{2}{\pi} \int_\alpha^\beta R^{-1} \sin(x/4R + Rt) \sinh[x(4R)^{-1} |(1 - 24R^2 + 16R^4)^{\frac{1}{2}}|] dR\right\} H(t+x). \tag{5.9}$$

Here the first term is the contribution from the pole at the origin while the integral is the contribution from the contours around the branch cuts. This method of de-

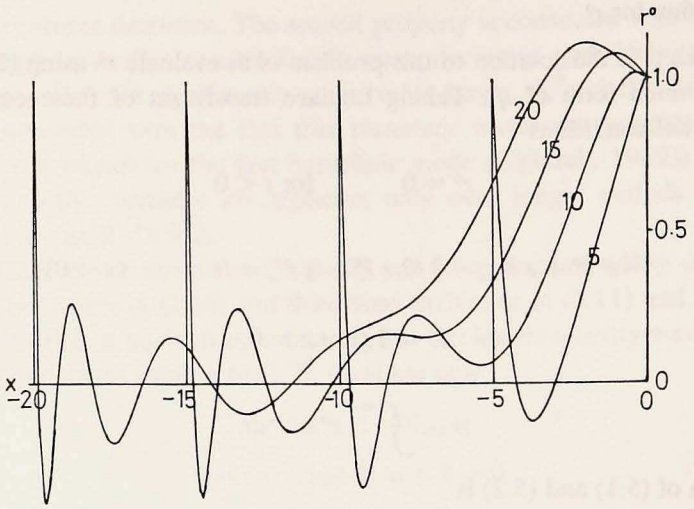

Figure 4. r^0 in the exact case as a function of x and t. The number attached to each curve is the time at which that solution occurs.

forming the contour of integration will be used to derive all the solutions given in this section and in §6. The solution (5.9) is drawn in Fig. 4 for various values of t; it can be seen to take the form of an initial disturbance traveling with unit velocity, in our nondimensional units, with a larger scale flow behind. It is tempting to interpret the first term in (5.9) as the planetary wave response as it is the contribution from $s = 0$, and the integral as a disturbance confined near the coast, as the range of integration is just the range of frequencies for which such disturbances exist in r^0 (see Fig. 2). That this is not the correct interpretation is seen from the fact that the initial disturbance travels with unit speed, a speed which can be attained only by inertia-gravity waves, and the initial discontinuity at $x + t = 0$ is entirely due to the first term in (5.9). That is, this first term certainly contains information about inertia-gravity waves. Similarly the decay of the initial disturbance just behind the discontinuity at $x + t = 0$ is due to the integral, which thus also contributes to the inertia-gravity waves. However, it can be seen that the integral becomes very small for $t >> -x$ due to the rapid oscillation of the factor $\sin(x/4R + Rt)$ and thus the first term in (5.9) gives the asymptotic behavior of r for $t >> -x$: $r^0 \sim 1$ as $t \to \infty$ at fixed x.

An interesting feature of Fig. 4 is the form of the discontinuity at the head of the solution. It can be seen that the inertia-gravity waves give rise to a frontogenetic effect, i.e. they increase the gradients just behind the head of the disturbance. This can be explained as follows. For large s, (5.7) becomes

$$r^0 \sim \frac{1}{2\pi i}\int_{\Gamma} s^{-1}\exp[x/2s + s(x+t)]ds. \tag{5.10}$$

Usually, letting s become large gives the nature of the solution for t small. However, (5.10) shows that in this case s large corresponds to $(x + t)$ small, i.e. in the vicinity of the head. Evaluating (5.10) gives

$$r^0 \sim J_0[(-2x(x+t))^{\frac{1}{2}}]\, H(x+t). \tag{5.11}$$

An interesting comparison can be made between (5.11) and the thinning western boundary layer given by Lighthill (1969), which has the form $1-J_0(\sqrt{2xt})$. If (5.11) is referred to a frame moving with speed -1 we obtain

$$J_0[(-2x(x+t))^{\frac{1}{2}}] = J_0[(2\xi(t-\xi))^{\frac{1}{2}}] \text{ where } \xi = x + t$$

$$\sim J_0[(2\xi t)^{\frac{1}{2}}] \text{ for } \xi << t. \tag{5.12}$$

Thus inertia-gravity waves produce strong gradients in the westward traveling disturbance in much the same way as short planetary waves traveling eastward from a stationary western boundary do.

6. The general solution for q^m ($m = 2, 4, 6, \ldots$)

From the transforms of (2.11), (2.14) and (2.15) we find that

$$q^m = A^m \exp(k^m{}_+ x) \tag{6.1}$$

where

$$k^m{}_+ = -(4s)^{-1} + (4s)^{-1}[1 + 16\,(m - \tfrac{1}{2})\, s^2 + 16s^4]^{\frac{1}{2}} \tag{6.2}$$

and the square root is defined to be positive for s real and positive. At $x = 0$ we have

$$q^m = A^m = (2s^2 + 2sk^m{}_+ + m)^{-1} A^{m-2} = \left[s \prod_{n=1}^{m/2} (2s^2 + 2sk^{2n}{}_+ + 2n) \right]^{-1}. \tag{6.3}$$

The integrand (6.1) has a series of branch points along the imaginary axis and a simple pole at the origin. The branch points of $k^m{}_+$ will be defined as $\pm i\,\alpha^m$, $\pm i\,\beta^m$ where α^m *and* β^m are the positive roots of $16\xi^4 - 16(m-\frac{1}{2})\,\xi^2 + 1 = 0$, and $\beta^m > \alpha^m$. If the branch cuts are taken from $i\alpha^m$ to $i\beta^m$ and from $-i\alpha^m$ to $-i\beta^m$ the integral may be written, using the same general method as in § 5, as

$$q^m = \frac{2}{\pi(m!)^{\frac{1}{2}}} \int_{\alpha^2}^{\beta^2} \left\{ \frac{1}{R} \sin\left(Rt + \frac{x}{4R}\right) \cos\phi \sinh\Phi + \frac{1}{R} \cos\left(Rt + \frac{x}{4R}\right) \right.$$

$$\left. \sin\phi \cosh\Phi \right\} dR$$

$$+\frac{2}{\pi(m!)^{\frac{1}{2}}}\sum_{r=1}^{m/2-1}(2r!)^{\frac{1}{2}}$$

$$\int_{a^{2r+2}}^{a^{2r}}\left\{\frac{\sin(Rt+x/4R)\cos\phi_r\sinh\Phi+\cos(Rt+x/4R)\sin\phi_r\cosh\Phi}{R\prod_{j=1}^{2}[-2R^2+2j-1/2+2(R^4-(2j-1/2)R^2+1/16)^{\frac{1}{2}}]}\right\}dR$$

$$+\frac{2}{\pi(m!)^{\frac{1}{2}}}\sum_{r=1}^{m/2-1}(2r!)^{\frac{1}{2}}$$

$$\int_{\beta^{2r}}^{\beta^{2r+2}}\left\{\frac{\sin(Rt+x/4R)\cos\phi_r\sinh\Phi+\cos(Rt+x/4R)\sin\phi_2\, r\cosh\Phi}{R\prod_{j=1}^{r}[-2R^2+2j-1/2-2(R^4-(2j-1/2)R^2+1/16)^{\frac{1}{2}}]}\right\}dR$$

$$+\left[\prod_{j=1}^{m/2}(2j)\right]^{-1} \tag{6.4}$$

$$\text{where } \phi=\sum_{j=1}^{m/2}\theta\,(m-2j+3/2) \tag{6.5}$$

$$\phi_r=\sum_{j=1}^{m/2-r}\theta\,(m-2j+3/2) \tag{6.6}$$

$$\theta(m-r)=\tan^{-1}\{[-1/16+(m-r)R^2-R^4]^{\frac{1}{2}}(2R^2-m+r)^{-1}\} \tag{6.7}$$

and

$$\Phi=\frac{x}{R}[-1/16+(m-1/2)R^2-R^4]^{\frac{1}{2}}. \tag{6.8}$$

7. The coastal Kelvin wave at the east

We now reconstruct the series for q as in (2.4). Owing to the complicated nature of (6.4) attention is confined to the coast, $x = 0$, although similar considerations would enable q to be reconstructed everywhere. We note that, from (2.5), $q = p$ at $x = 0$ and so at the coast the reconstructed q is just the pressure anomaly. The sum $q = D_0(y) + \sum_{m=2,4,\ldots}^{\infty} q^m D_m(y)$ at $x = 0$ is reconstructed in Fig. 5 for various values of t. (The term $D_0(y)$ is due to the incident equatorial Kelvin wave.) The initial peak is seen to amplify as it travels away from the equator; from measurements of this figure it is apparent that it amplifies as $y^{\frac{1}{4}}$. On a mid-latitude β-plane an analysis similar to that of Moore (1968) (Ch. IV) shows that for high frequencies the coastal Kelvin wave is confined to within a distance $\propto 1/y$, independent of frequency, of the coast. The initial behavior of the solution is given by the behavior of the Laplace transform for large s, which corresponds to high frequencies. Thus the initial disturbance of our coastal Kelvin wave is confined within a distance

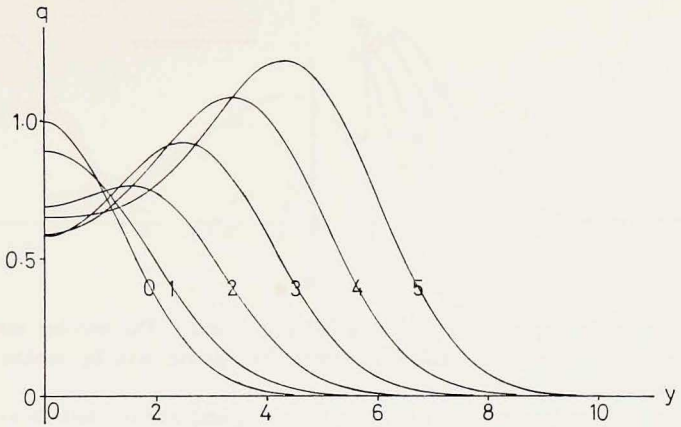

Figure 5. The coastal Kelvin wave, q at $x = 0$, as a function of y and t in the exact case. The number attached to each curve is the time at which that solution occurs.

$\propto 1/y$, independent of t, of the coast. Although, in general, the energy of the coastal wave is not rigorously conserved (nor even rigorously defined) for short times, the loss to planetary waves and inertia-gravity waves beyond the radius of deformation of the coast may be neglected. Conservation of energy then suggests that this initial disturbance must amplify as $y^{\frac{1}{2}}$ as it propagates away from the equator, thus explaining the observed behavior.

The integrals in (6.4) decay fairly rapidly with time, and q^m soon becomes

$$q^m = \left[\prod_{j=1}^{m/2} (2j) \right]^{-1} . \tag{7.1}$$

At fixed y we then have

$$q \sim D_0(y) + \sum_{m=2,4,6\ldots}^{\infty} \left[\prod_{j=1}^{m/2} (2j) \right]^{-1} D_m(y). \tag{7.2}$$

but this series is just the expansion of $2^{-\frac{1}{2}}$ in parabolic cylinder functions. Thus we have

$$q \sim 2^{-\frac{1}{2}} \text{ as } t \to \infty. \tag{7.3}$$

Hence at any latitude the pressure anomaly eventually becomes equal to the magnitude of the incident equatorial Kelvin wave divided by $2^{\frac{1}{2}}$ (for an incident wave of step-function form). From Fig. 4 it can be seen that the initial disturbance in the coastal Kelvin wave travels with unit speed in our nondimensional units, as it is expected to do since we have used the speed (c_n) of coastal Kelvin waves in our nondimensionalization.

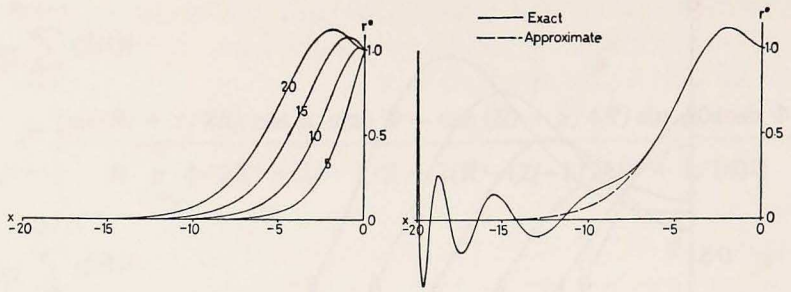

Figure 6. (left) r^0 in the approximate case as a function x and t. The number attached to each curve is the time at which that solution occurs. Evaluation was by means of series (8) summed to 50 terms.

Figure 7. (right) Comparison of r^0 at $t = 20$ in the exact and approximate cases. For $x > -7$ the curve are effectively identical.

8. An approximate solution

Using the filtered versions of (2.9) and (2.11-2.14), the solution for r^0 is

$$r^0 = \frac{1}{2\pi i}\int_{\Gamma} \frac{e^{\kappa x + st}}{s}\, ds \tag{8.1}$$

where

$$\kappa = -\frac{1}{4s} + \left(\frac{1}{16s^2} + 3/2\right)^{\frac{1}{2}} .$$

Evaluation of (8.1) is possible by direct integration as in § 5 with branch cuts from $s = \pm\, i/2\sqrt{6}$ to $\pm\, i\,\infty$ but the integrals converge less rapidly in this case than in § 5 and so an alternative method is adopted here. If we define

$$z = 2(6)^{\frac{1}{2}}\, s - (1 + 24s^2)^{\frac{1}{2}} \tag{8.2}$$

then (8.1) becomes

$$r^0 = \frac{1}{2\pi i}\int_{\Gamma_1} \frac{(1+z^2)}{z(1-z^2)} \exp\left\{\frac{(z^2-1)}{4(6)^{\frac{1}{2}}z}\, t + (3/2)^{\frac{1}{2}} \times \left(\frac{1+z}{1-z}\right)\right\} dz \tag{8.3}$$

where Γ_1 is a circle surrounding the origin, and the integration proceeds anticlockwise. The integrand may be expanded as a Laurent series about $z = 0$ and r^0 is then just the coefficient of z^{-1} in this expansion. The first few terms in expansion for r^0 are

$$r^0 = \exp[(3/2)^{\frac{1}{2}}\, x]\, \{J_0(\tau) - 6^{\frac{1}{2}}\, x\, J_1(\tau) + (2 + 6^{\frac{1}{2}}\, x + 3x^2)\, J_2(\tau) - \ldots\} \tag{8.4}$$

where $\tau = t/2(6)^{\frac{1}{2}}$ and use has been made of the generating function for Bessel functions

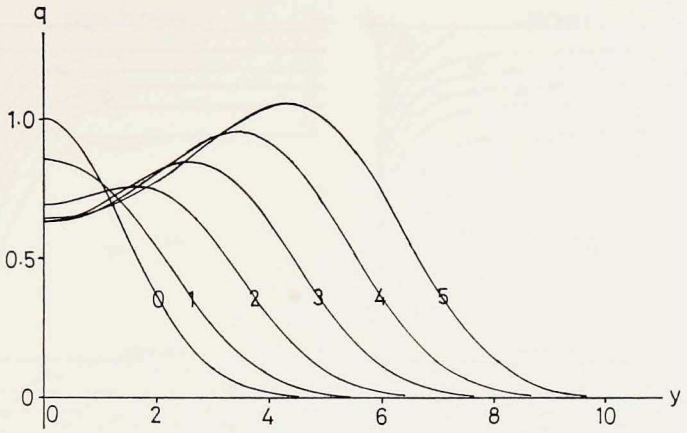

Figure 8. The coastal Kelvin wave, q at $x = 0$, as a function of y and t in the approximate case with the exact recurrence relation 2.14. The number attached to each curve is the time at which that solution occurs.

$$\exp\left\{\frac{t}{4(6)^{\frac{1}{2}}}\left(z-\frac{1}{z}\right)\right\} = \sum_{k=-\infty}^{\infty}(-z)^k J_{-k}\left(\frac{t}{2(6)^{\frac{1}{2}}}\right). \tag{8.5}$$

Fig. 6 is a plot of r^0 obtained from (8.4) when fifty terms are included in the summation.

Comparison with Fig. 4 shows that behind the initial inertia-gravity wave disturbance, in the region dominated by planetary waves, the approximate solution agrees closely with that for the exact case. Of course the approximation cannot hope to give good results in the region of the head of the disturbance as we have explicitly removed inertia-gravity waves in this solution by our filtering process. For a better comparison the exact and approximate curves for $t = 20$ are superimposed in Fig. 7, where they are seen to be in remarkably good agreement in the region dominated by planetary waves.

9. The eastern coastal Kelvin wave in the approximate case

The method of § 8 can be extended to general m provided a suitable boundary condition is available. In the Appendix it is shown that the best boundary condition is (2.14) with r^m set equal to q^m. Equation (2.14) can be simplified by dropping the second time derivative. This leads to some loss of amplitude in the vicinity of the head of the Kelvin wave but is otherwise acceptable.

The solution is plotted in Fig. 8. The agreement with Fig. 5 is good except that the amplitude of the head is slightly less, though the speed of propagation is not affected.

It seems plausible that the reason for this approximation giving a coastal Kelvin

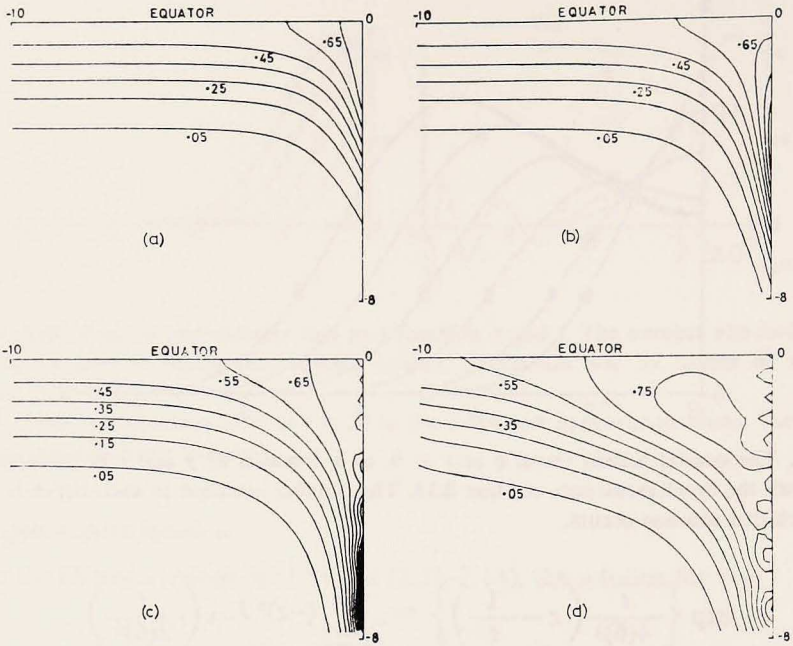

Figure 9. Contours of the p field at $t = 2, 4, 8, 20$ respectively. The contour interval is .1. The .05 contour is farthest south. The distortion of the p field by the coastal wave is apparent as is the southerly propagation of the disturbance. Northern hemisphere contours are not drawn since the solution is symmetric with respect to the equator. The x-scale is from 0 to -10, and the y-scale from 0 to -8. The oscillations at the coast result from having a finite number of parabolic cylinder functions (28) in the expansion.

wave very similar to that in the exact solution is that the meridional dependence of the equatorial Kelvin waves is smooth and so the coastal wave has no sudden discontinuity in the vicinity of its head. This implies that high frequencies are not present in this coastal Kelvin wave and so the approximation, being good for low frequencies, gives good agreement with the exact solution. This should be contrasted with the solution for r^0 as a function of x and t at $y = 0$, which in the exact solution has an initial discontinuity which does not appear at all in the approximate solution.

10. The solution away from the boundary

Using the approximation of sections 8 and 9, it is possible to construct an efficient numerical model of the equations where the east-west variation is expressed in terms of Chebyshev polynomials (Anderson, 1974). Contour plots of p, u, v from this model of times, 2, 4, 8, 20 are shown in Figs. 9, 10, 11 respectively. The incoming equatorial Kelvin wave is included though the mechanism of its generation is not. (For example, the equatorial Kelvin wave could be set up at the western boundary

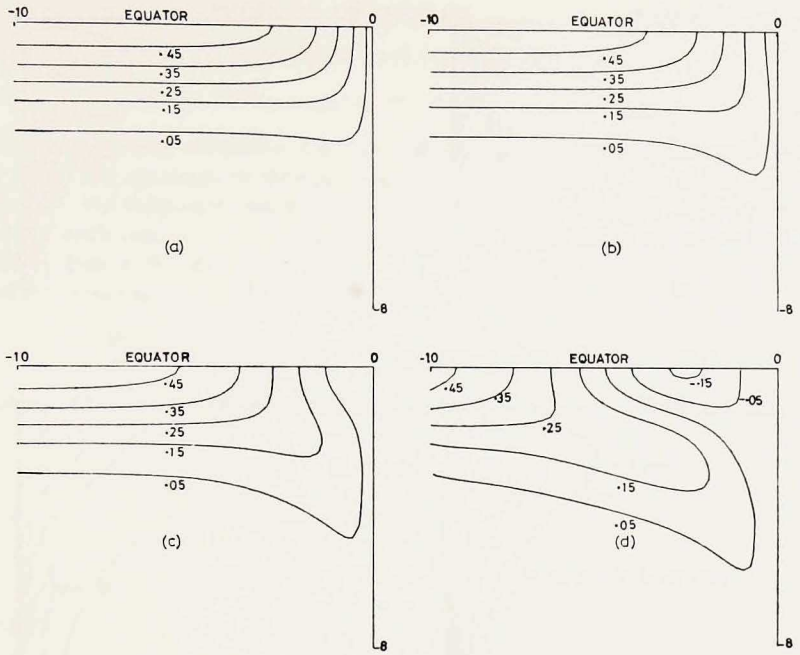

Figure 10. As for Fig. 9, but for u. The reflected waves act to cancel out the incoming Kelvin wave and by $t = 20$, weak westward velocities have been established along the equator.

by planetary waves of exactly the same form as those activated by the Kelvin wave at the eastern boundary since the equations are invariant to reversal of x and t).

Fig. 9 shows how the pressure field is distorted by the coastal Kelvin wave. (Initially the isobars are parallel to the equator). The movement of the head of the Kelvin wave along the boundary away from the equator is clearly illustrated in Figs. 9a, 9b, 9c. By $t = 20$ the head of the Kelvin wave is well out of the region of interest. Initially the coastal wave produces strong gradients in the vicinity of the coast but planetary waves propagate the front westward leaving a fairly flat field behind (asymptotically of amplitude $2^{-\frac{1}{2}}$ of the initial field). Fig. 10 illustrates the same features, and shows how the reflected waves cancel out the velocity field set up by the initial equatorial Kelvin wave. By $t = 20$, in fact, a weak westward flow has been set up near the equator. The meridional velocity in Fig. 11 can be thought of as being due entirely to coastal influences, since for the equatorial Kelvin wave v is identically zero. For low latitudes there is initially a strong coastal current set up but as the planetary waves travel westward, the velocity near the coast declines, and by $t = 20$, when the pressure field is fairly flat, the velocity near the coast is very small. As the frontal zone travels westward the associated velocity decreases. This is because the velocity field is geostrophic to the pressure field and the frontal zone weakens as it travels westward.

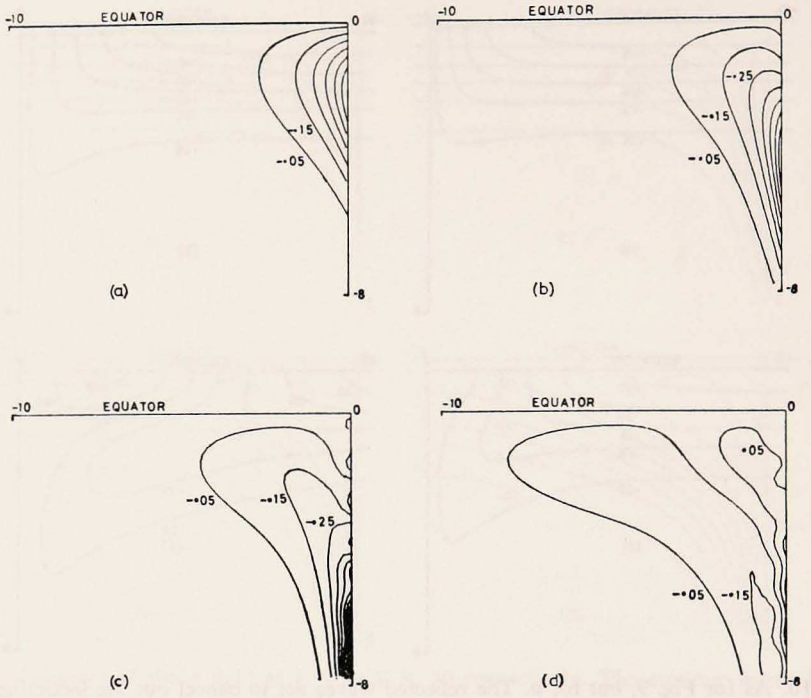

Figure 11. As for Fig. 9, but for v. The incoming equatorial wave has v identically zero.

11. Summary

We have shown how a step-function equatorial Kelvin wave incident on an eastern meridional oceanic coast generates reflected planetary waves and coastal Kelvin waves. The low frequency approximation of § 8 gives a coastal Kelvin wave which is in good agreement with that in the exact case. The reflected planetary waves are approximated well in the region behind the initial inertia-gravity wave disturbance. These results give some idea of the confidence which might be placed in approximate solutions to other equatorial problems with meridional boundaries, for example the flow generated by a suddenly imposed wind-stress. In general the coastal Kelvin wave would be expected to be well approximated in most problems. Also, the reflected planetary waves would be well approximated but the initial inertia-gravity wave disturbance in the reflected wave would not. The techniques used to evaluate both the exact and approximate solutions are immediately applicable to these other problems.

Acknowledgments. The authors wish to thank Drs. A. E. Gill and M. E. McIntyre for helpful discussions during the preparation of this paper. This work was supported by a N.E.R.C. fellowship (DLTA) and a N.E.R.C. studentship (PBR).

APPENDIX

For the exact eqs. (2.9-2.12) either (2.13), or (2.14) or the alternative

$$2r^m{}_{tt} - 2r^m{}_{xt} + (m+1)\, r^m - (m+1)(m+2)\, q^{m+2} = 0 \tag{A1}$$

can be used as boundary conditions, together with (2.15). They are in all respects equivalent. However, when the approximate versions of (2.9-2.12) are solved, (2.13), (2.14) and (A1) are not equivalent. The long-term behavior of the solution will be obtained correctly by the use of any of the equations, but for short times (2.14) gives results which are much closer to the exact solution than do the others.

The ratio of terms in the exact case is, from (6.3)

$$\frac{A^{m+2}}{A^m} = \{2s^2 - \tfrac{1}{2}[1 - (1 + 16\,(m+3/2)s^2 + 16s^4)^{\frac{1}{2}}] + m + 2\}^{-1} \tag{A2}$$

whereas, using (2.14) in the approximate case it is

$$\frac{A^{m+2}}{A^m} = \{2s^2 - \tfrac{1}{2}\,[1 - (1 + 16\,(m+3/2)\,s^2)^{\frac{1}{2}}] + m + 2\}^{-1}\ . \tag{A3}$$

For (2.13) in the approximate case it is

$$\frac{A^{m+2}}{A^m} = [1 - s^2/(m+1)]\ \{m + 3/2 + s^2 + \tfrac{1}{2}\ [1 + 16\,(m + 3/2)\,s^2]^{\frac{1}{2}}\}^{-1} \tag{A4}$$

and for (A1) it is

$$\frac{A^{m+2}}{A^m} = \left[1 + \frac{4s^2}{(m+1)(m+2)}\right]\left\{2s^2 + m + 3/2 + \tfrac{1}{2}\,[1 + 16\,(m + 3/2)\,s^2]^{\frac{1}{2}}\right\}^{-1}\ . \tag{A5}$$

In the limit $s \to 0$, (A3-A5) all converge to the correct results (A2), but in the limit $s \to \infty$, this is not true.

(A2) $\to$ $1/4s^2$

(A3) $\to$ $1/2s^2$

(A4) $\to$ $-1/(m+1)$

(A5) $\to$ $\dfrac{2}{(m+1)(m+2)}$

Thus it can be seen that (A4), and (A5) will do very badly since they will lead to all components being activated immediately. (A3) will give the correct temporal development though not of quite the correct magnitude. In section (9), it is thus eq. (2.14) which is used as boundary condition, and the approximate solution using this eq. is given in Fig. 8 for contrast with the exact solution of Fig. 5.

REFERENCES

Abramowitz, M., and Stegun, I. A. 1965. Handbook of Mathematical Functions. Dover, 1046 pp.

Anderson, D. L. T. 1974. A low latitude ocean spectral model using Chabyshev-parabolic cylinder functions. (Garp Programme on Numerical Experimentation W.G.N.E.) Report No. 7.

Blandford, R. 1966. Mixed gravity-Rossby waves in the ocean. Deep-Sea Res., *13*, 941–961.

Bretherton, F. P. 1965. Woods Hole Geophysical Fluid Dynamics lectures.

Erdelyi, A., Magnus, W., Oberhettinger, F., Tricomi, F. G. 1954. Tables of integral transforms, Vol. 1. New York, McGraw-Hill, 391 pp.

Fjortoft, R. 1962. On the integration of a system of geostrophically balanced prognostic equations. Proceedings of the International Symposium on Numerical Weather Prediction 153–159, Meteorological Society of Japan, Tokyo.

Gill, A. E. 1973. Models of equatorial currents. Proceedings of "Numerical Models of Ocean Circulation", symposium in Durham, N.H. 1972. U.S. National Academy of Sciences.

Gill, A. E., and Clarke, A. J. 1974. Wind-inducing upwelling, coastal currents and sea-level changes. Deep-Sea Res., *21*, 325–346.

Ichiye, T. 1959. On long waves in a stratified, equatorial ocean caused by a travelling disturbance. Deep-Sea Res., *6*, 16–37.

Lighthill, M. J. 1969. Dynamic response of the Indian Ocean to onset of the southwest monsoon. Philosophical Transactions of the Royal Society of London *A 265*, 45–92.

Mofjeld, H. O., and Rattray, M. Jr. 1971. Free oscillations in a beta-plane ocean. J. Mar. Res., *29*, 281–305.

Moore, D. W. 1968. Planetary-gravity waves in an equatorial ocean. Ph.D. dissertation, Harvard University, Cambridge, Massachusetts, 207 pp.

Veronis, G., and Stommel, H. 1956. The action of a variable wind-stress on a stratified ocean. J. Mar. Res., *15*, 43–75.

Walin, G. 1972. On the hydrographic response to transient meteorological disturbances. Tellus, *24*, 1–18.

Yanai, M., and Maruyama, T. 1966. Stratospheric wave disturbances propagating over the tropical Pacific region. Journal of the Meteorological Society of Japan, *44*, 291–294.

Yoshida, K. 1959. A theory of the Cromwell Current (the equatorial undercurrent) and of the equatorial upwelling—An interpretation in a similarity of a coastal circulation. Journal of the Oceanographic Society of Japan, *15*, 1–12.

Received: *10 November, 1975;* revised: *19 February, 1976.*